Available online at www.sciencedirect.com
ScienceDirect
Journal of Molecular Catalysis A: Chemical 265 (2007) 167–176
JOURNAL OF MOLECULAR CATALYSIS A: CHEMICAL
www.elsevier.com/locate/molcata

Effect of the silica texture on grafting metallocene catalysts

Fernando Silveira [a], Gilvan P. Pires [a], Cristiane F. Petry [a], Dirce Pozebon [a], Fernanda C. Stedile [a], João H.Z. dos Santos *, Arnaud Rigacci [b]

[a] *Instituto de Química, Universidade Federal do Rio Grande do Sul (UFRGS), Av. Bento Gonçalves 9500, Porto Alegre 91501-970, Brazil*
[b] *École des Mines de Paris, Center for Energy and Processes (CENERG), BP 207, F-06904 Sophia, Antipolis Cedex, France*

Received 8 August 2006; received in revised form 4 October 2006; accepted 5 October 2006
Available online 12 October 2006

Abstract

A series of hybrid supported catalysts was prepared by sequentially grafting Cp_2ZrCl_2 and $(n\text{BuCp})_2ZrCl_2$ (1:3 ratio) onto synthesized xerogel, aerogel and commercial silicas. Supports and catalysts were characterized by Rutherford backscattering spectrometry, energy-dispersive X-ray scanning electron microscopy, atomic force microscopy and nitrogen adsorption. Grafted metal content laid between 0.15 and 0.5 wt.% Zr/SiO_2. All the systems were shown to be active in ethylene polymerization with methylaluminoxane as the co-catalyst. Catalyst activity and molecular weight were shown to depend on the textural characteristic of the silicas, namely grain size and pore diameter. The highest activity in ethylene polymerization (ca. 5310 kg PE mol Zr^{-1} h^{-1}) was obtained with the supported catalyst using commercial silicas with average particle size around 50 μm. Particles with sizes of 80–90 μm obtained less activity. Resulting polymers were characterized by gel permeation chromatography and differential scanning calorimetry.

Keywords: Supported metallocenes; Silica; Sol–gel; Polymerization; AFM

1. Introduction

In the last 15 years much research has been devoted to the development of supported metallocenes. Metallocene, due to its single-site catalyst nature, allows the production of tailored polymers in terms of molecular weight, molecular weight distribution, stereoregularity, and comonomer incorporation. Such polymers, with narrow molecular weight distribution, have improved physical properties such as impact and environmental crack resistance and clarity. Nevertheless, these polymers impinge some technological constraints in terms of processing due to its narrow molecular weight distribution. Broad molecular weight distribution affords higher fluidity in the molten state at high shear rates, particularly in extrusion processes. Some strategies to broaden molecular weight distribution of polymers produced by single-site catalysts are: (i) blend polymers produced by individual catalysts; (ii) use of multireactor technology; (iii) use of tandem catalysts in a single reactor [1].

The combination of two different metallocenes on the same support has been investigated in the literature as a strategy which aims at overcoming the two above-mentioned constraints of metallocene catalysts: the necessity of development of supported catalysts and the potentiality of broadening of the molecular weight distribution [1]. For instance, the combinations of metallocenes such as $EtInd_2ZrCl_2$ and Cp_2ZrCl_2 [2] or Cp_2NbCl_2 and $(n\text{BuCp})_2ZrCl_2$ [3] have already been reported in the literature. In a previous work, we reported the effect of combining Cp_2ZrCl_2 and $(n\text{BuCp})_2ZrCl_2$ on the same silica support, grafted in different addition orders and molecular ratios, on catalyst activity and on polymer properties. The best catalyst was that obtained by grafting Cp_2ZrCl_2 followed by $(n\text{BuCp})_2ZrCl_2$ in 1:3 ratio [4,5]. In a sequel to this work, we investigated the effect of the nature of silica on sequentially grafting these two metallocenes.

A few studies dealt with the effect of silica texture on supported metallocene systems. Metallocene supported on high pore diameter microspherical silicas give polyethylene with high activity and good polymer morphology [6]. Harrison et al. [7] studied the effect of different silicas (and alumina), chemically modified with MAO, on the heterogenization of en-

* Corresponding author. Tel.: +55 51 3316 7238; fax: +55 51 3316 7304.
E-mail address: jhzds@iq.ufrgs.br (J.H.Z.d. Santos).

1381-1169/$ – see front matter © 2006 Elsevier B.V. All rights reserved.
doi:10.1016/j.molcata.2006.10.008

$(Ind)_2ZrCl_2$, $Me_2Si(Ind)_2ZrCl_2$ and $Me_2C(Cp)(Flu)ZrCl_2$ on catalyst activity and on molecular weight of the resulting polymers. The results suggest influences of the texture of the supports on the properties of the resulting polymers. Fink's group [8] investigated the effect of silica particle size in supported *rac*-$Me_2Si(IndR_2)_2ZrCl_2$ on catalyst activity in propylene polymerization and on polymer molecular weight and molecular weight distribution. The authors concluded that the catalyst particles with small-sized silica afforded an increase of the polymerization rate due to the uniform distribution of the MAO co-catalyst on the surface, which led to polymers with larger molecular weight. Cp_2ZrCl_2 was immobilized on commercial silicas, bearing different surface area and pore diameter. The determination of adsorption isotherm showed that maximum grafted content was observed in the case of high surface area (Silica Grace 948). No influence of pore diameter on Zr content was detected [9].

In the present paper, Cp_2ZrCl_2 and $(n\text{BuCp})_2ZrCl_2$, in a 1:3 ratio, were grafted on a silica support by sol–gel and precipitation methods. The resulting catalyst was characterized by Rutherford backscattering spectrometry (RBS), Energy-dispersive X-ray scanning electron microscopy (EDX-SEM), atomic force microscopy (AFM) and nitrogen adsorption. The resulting hybrid supported catalysts were evaluated in ethylene polymerization, with MAO as co-catalyst. The polymers were characterized by gel permeation chromatography (GPC) and differential scanning calorimeter (DSC).

2. Experimental

2.1. Materials

All the chemicals were manipulated under inert atmosphere using the Schlenk technique. Silica Grace 948, 955 and 956 were activated under vacuum ($P < 10^{-5}$ bar) for 16 h at 450 °C. $(n\text{BuCp})_2ZrCl_2$ (Aldrich), Cp_2ZrCl_2 (Aldrich), $Si(OEt)_4$ (Merck), $SiCl_4$ (Merck), $ZrCl_4$ (Aldrich) and MAO (Witco, 10.0 wt.% toluene solution) were used without further purification. Ultrapure water (resistivity of 18.2 MΩ cm) from a Milli-Q® (Bedford, USA) purifier system and HNO_3 (Merk) were used for calibration solutions and Zr determination by ICP OES. Calibration solutions ranging from 5 to 15 μg L^{-1} of Zr were prepared in 10% (v/v) HNO_3 by serial dilutions of a 1000 mg L^{-1} Zr stock solution (Titrisol®, Merck). The gases used in the ICP OES spectrometer were compressed air as chear gas, nitrogen (purity of 99.996%) as purge gas of the optic system, and argon (purity of 99.996%) as principle, auxiliary and nebulizer gas. The gases used were from White Martins/Praxair, Basil. Pure ethylene and argon (from White Martins/Praxair) were passed through molecular sieve columns for purification and drying.

2.2. Synthesis of xerogel and aerogel silicas

Two xerogels were synthesized: one through a hydrolytic acid route and another one through a non-hydrolytic route.

2.2.1. Synthesis of silica xerogel by hydrolytic acid route [10,11]

Tetraethylorthosilicate ($Si(OEt)_4$) and HNO_3 (0.3 M) were poured together into a glass reactor and vigorously stirred at room temperature. H_2O:$Si(OEt)_4$ volume ratio was kept under 2. Initially, the mixture was separated in two phases. When the mixture was stirred, an emulsion was formed and water was dispersed as droplets. After 3–10 min a homogeneous solution was formed. In the following days, viscosity increased and a solid transparent monolith was obtained. The resulting xerogel (6.30 g) was washed with acetone and dried at 140 °C for 3 days.

2.2.2. Synthesis of silica xerogel by non-hydrolytic route [12,13]

Equimolar amounts of $Si(OEt)_4$ (0.024 mol) and $SiCl_4$ (0.024 mol) were mixed in toluene in the presence of $ZrCl_4$ (acid Lewis catalyst) and heated at 90 °C for 20 min. The resulting monolith (3.65 g) was washed in acetone and the product dried under vacuum for 3 days.

2.2.3. Synthesis of silica aerogel

Silica aerogel was synthesized by the sol–gel method under supercritical conditions at CENERG (France). Experimental conditions are described elsewhere [14].

2.3. Synthesis of supported hybrid catalysts

Cp_2ZrCl_2 toluene solution corresponding to 0.25 wt.% Zr/SiO_2 was added to ca. 1.0 g of pre-activated silica and let stirring for 30 min at room temperature. The solvent was removed under vacuum through a fritted disk. A $(n\text{BuCp})_2ZrCl_2$ toluene solution corresponding to 0.75 wt.% Zr/SiO_2 was added and the resulting slurry was stirred for 30 min more at room temperature, and then filtered through a fritted disk. The resulting solids were washed with 15× 2.0 cm^3 of toluene and dried under vacuum for 4 h.

The procedure above was used for the several silicas used in this work (Grace 956, 955 and 948, xerogel silica by non-hydrolytic route, xerogel silica by hydrolytic route and aerogel silica). These silicas generated the heterogeneous catalytic systems after grafting, respectively: G56, G55, G48, NHY, HYD and AER.

2.4. Characterization of silicas and supported catalysts

2.4.1. Elemental analysis (CHN)

Carbon content was determined in a Perkin-Elmer M-CHNSO/2400 analyzer.

2.4.2. Rutherford backscattering spectrometry (RBS)

Zirconium loadings in catalysts were determined by RBS using He^+ beams of 2.0 MeV incident on homogeneous tablets of the compressed (12 MPa) powder of the catalyst systems. The method is based on the determination of the number and energy of the detected particles, which are elastically scattered in the Coulombic field of the atomic nuclei in the target. In this study, the Zr/Si atomic ratio was determined by the heights of

the signals corresponding to each of the elements in the spectra and converted to wt.% Zr/SiO_2. For an introduction to the method and applications of this technique the reader is referred elsewhere [15].

2.4.3. Nitrogen adsorption–desorption isotherms

Samples were previously degassed (10^{-2} mbar) at 120 °C (silica) or at 85 °C (supported catalysts) for 8 h. Adsorption–desorption nitrogen isotherms were measured at −196 °C in a Gemini 2375 (Micromeritics). Specific surface area (S_{BET}) were determined by the Brunauer–Emmett–Teller equation ($P/P_0 = 0.05$–0.35). The mesopore size and distribution were calculated by the Barrett–Joyner–Halenda (BJH method) using the Halsey standards. Desorption branch was used. Micropore volumes were calculated by the *t*-plot method, using the Harkins and Jura standard isotherm.

2.4.4. Surface coverage concentration

Surface coverage concentration ($\Gamma = \mu mol\ m^{-2}$) was calculated taking into account the model proposed by Amati and Kováts [16], employing data from elemental analysis (carbon content) and by nitrogen adsorption (specific surface area), according to Eq. (1):

$$\Gamma = \frac{10^6}{S_{BET}}\left(\frac{1201 \times n\mathrm{C}}{\%C_{CHN}} - M_{SUB} + \delta\right)^{-1} \quad (1)$$

where S_{BET} ($m^2\ g^{-1}$) is the specific surface area of the untreated silica, *n*C the number of atoms of carbon of the surface coverage substituent, M_{SUB} the molecular mass of the substituent (in this case, the supported metallocene), and δ is the correction for desorbed water and the proton substituted during reaction. In the present study, $\delta = 1$.

2.4.5. Atomic force microscopy (AFM)

Images of silica and supported catalyst surfaces were obtained using an Atomic Force Microscopy, Nanoscope IIIa®, manufactured by Digital Instruments Co., using the contact mode technique with probes of silicon nitride. WS M 4.0 software from Nanotec Electronic S.L. was used for the images treatment. Samples were compressed in the form of tablets and fragments of roughly 16 mm^2, which were employed for the analysis.

2.4.6. Scanning electron microscopy (SEM) and energy dispersive X-ray (EDX)

SEM and EDX experiments were carried out on a JEOL JSM/6060 and JEOL JSM/5800, respectively. The catalysts were initially fixed on a carbon tape and then coated with gold by conventional sputtering techniques. The employed accelerating voltage was 10 kV for SEM and 20 kV for EDX.

2.5. Leaching test

The same amount (ca. 0.02 g) of the supported catalysts used in the slurry polymerization was put into contact with 0.150 L of MAO toluene solution MAO (Al/Zr = 1000) and transferred under argon into the fritted disk flask and stirred at 60 °C for 30 min. Subsequently, the slurry was filtered through the fritted disk and the eluent was concentrated to dryness. The flask was rinsed with small aliquots of 10% (v/v) HNO_3, which were transferred to a graduated polyethylene flask to a total volume of 50 mL. The Zr content of the eluent was then determined by inductively coupled plasma optical emission spectrometry (ICP OES) by using an Optima 2000 DV Perkin-Elmer instrument. The sample introduction system was composed of a Scott® spray chamber and a GemCone® nebulizer, both coupled to an alumina injector. Zirconium was measured through the axial view of the plasma. The other parameters used were those recommended by the instrument manufacturer.

2.6. Polymerization reactions

Polymerizations were performed in toluene (0.15 L) in a 0.30 L Pyrex glass reactor connected to a constant temperature circulator equipped with mechanical stirring and inlets for argon and monomers. For each experiment, a mass of catalyst system corresponding to 10^{-5} mol L^{-1} of Zr was suspended in 0.01 L of toluene and transferred into the reactor under argon. The polymerizations were performed at atmospheric pressure of ethylene at 60 °C for 30 min at Al/Zr = 1000, using MAO as a co-catalyst. Acidified (HCl) ethanol was used to quench the processes, and reaction products were separated by filtration, washed with distilled water, and finally dried under reduced pressure at 60 °C.

2.7. Polyethylene characterization

Molar masses and molar mass distributions were investigated with a Waters CV plus 150C high-temperature GPC instrument, equipped with viscosimetrical detector, and three Styragel HT type columns (HT3, HT4 and HT6) with exclusion limit 1×10^7 for polystyrene. 1,2,4-Trichlorobenzene was used as the solvent, at a flow rate of 1 $cm^3\ min^{-1}$. The analyses were performed at 140 °C. The columns were calibrated with standard narrow molar mass distribution polystyrenes and with linear low-density polyethylenes and polypropylenes.

Polymer melting points (T_m) and crystallinities (χ_c) were determined on a TA Instrument DSC 2920 differential scanning calorimeter connected to a thermal analyst 5000 integrator and calibrated with indium, using a heating rate of 20 °C min^{-1} in the temperature range of 30–150 °C. The heating cycle was performed twice, but only the results of the second scan are reported, because the former is influenced by the mechanical and thermal history of the samples.

3. Results and discussions

The silica surface, at least for moderate activation temperatures, is mainly composed of isolated and, to a lesser extent, of vicinal and geminal hydroxyl groups, as well as relatively unreactive siloxane bridges [17]. Silanol groups are capable of reacting with sequestering agents such as organometallic chlorides and alkoxides, with elimination of one or more of the original ligands. In the present case, zirconocenes are grafted

Table 1
Grafted metal loading of the resulting supported systems

Catalyst system	Zr/SiO_2 (wt.%)	*C* (%)	C/Zr
G56	0.5	1.81	28
G55	0.3	1.10	28
G48	0.4	1.65	31
HYD	0.5	1.82	28
NHY[a]	0.4	0.82	16
AER	0.15	0.78	40

[a] $ZrCl_4$ was used as Lewis acid catalyst during the synthesis, resulting a total of 12.9 wt.% Zr/SiO_2 in the support. The Zr content here reported refers to that from the zirconocene counterpart.

on the silica surface by elimination of the chloride ligand with hydrogen atoms from the silanol groups, leading to the formation of surface species.

Table 1 reports the grafted metal content determined by RBS and carbon content for the different supported systems resulting from the immobilization of Cp_2ZrCl_2 and $(n\text{BuCp})_2ZrCl_2$ on commercial and synthesized silicas.

According to Table 1, grafted metal content lies between 0.15 and 0.5 wt.% Zr/SiO_2. Metal loadings around 0.4 wt.% Zr/SiO_2 were already reported for such zirconocene grafted on silica support [18]. In the case of aerogel (AER), a very low Zr content was detected. Carbon content laid between 0.7 and 1.9%. Considering the 1:3 ratio (Cp_2ZrCl_2; $(n\text{BuCp})_2ZrCl_2$), the expected C/Zr ratio was expected to be 16. For all systems, this value was higher than 16, suggesting that Cp moieties might be kept during grafting reaction. Higher C/Zr ratio might be due to adventitious carbon present in the resulting catalyst.

It is worth noting that the different grafted content observed for such silicas could be due to a different number of silanol groups available on the support surface. It is generally believed that such silanol density is a function of thermal treatment, independent of the nature of silica support [19]. Nevertheless, Bergna [20] pointed out that the structure of silica surface is strongly dependent on the method of preparation. Differences observed in the literature in terms of silanol number were attributed to the presence of internal silanols and to a very heterogeneous distribution of hydroxyls resulting from the synthetic route [21].

The leachability of the grafted surface species was evaluated by submitting the catalyst to MAO contact under polymerization conditions, followed by filtration. The Zr content in the eluent was measured by ICP OES. According to Table 2, very low Zr amount (4–8 $\mu g\,L^{-1}$) was detected, suggesting that leaching is practically negligible in such systems.

Table 2
Zr concentration in the eluate from the supported catalysts

Samples	Leached Zr ($\mu g\,L^{-1}$)
G56	4.13
AER	<LOD
NHY	<LOD
HYD	7.27

LOD: limit of detection = 3.0 $\mu g\,L^{-1}$.

The shape of nitrogen isotherms and the hysteresis loops from the catalytic systems provide information about the shape of pores and slits-shaped pores on the catalyst surface. Fig. 1 shows the nitrogen adsorption–desorption isotherms for the six supported catalysts.

According to Fig. 1, the isotherms correspond to those of type IV in the BDDT classification, which is typical of mesoporous materials [22]. The most characteristic feature of type IV isotherm is the hysteresis loop, which is associated with the occurrence of pore condensation. The limiting uptake of nitrogen over a range of high P/P_0 results in a plateau of the isotherm, which indicates complete pore filling.

According to IUPAC classification, the hysteresis loop of G56, G55, G48 and AER isotherms are of type H1, which are often associated with porous materials consisting of well-defined cylindrical-like pore channels or agglomerates of compacts of approximately uniform spheres separated by slits. The hysteresis loop of HYD and NHY is of the type H4, with loops associated with narrow slit pores. The plateau observed at relative pressures higher than 0.8 indicates that large mesopores (pore diameter around 20 and 500 Å) are absent, leading to rather narrow pore size distributions.

Specific area of the silicas was also determined by nitrogen adsorption before and after zirconocene grafting (Table 3). The three commercial silicas presented surface area in the range of 210–265 $m^2\,g^{-1}$. The xerogel prepared by the non-hydrolytic method has specific area close to 200 $m^2\,g^{-1}$, while that prepared by the hydrolytic route, about 650 $m^2\,g^{-1}$. Aerogel presents typical high specific area intrinsic to these materials, which are dried under supercritical conditions [23].

For the systems G56, G55 and G48, i.e., supported zirconocenes on the commercial silica, there was a reduction in the specific surface area around 6% when comparing data before and after grafting. However, the micropore surface area reduced 13% for G56, 20% for G55 and 60% for G48. Such results suggest that grafting might also have been taking place inside the pores.

For the supported systems on xerogels, in the HYD system, the specific surface area is almost totally given by the micropore surface area. There is reduction of ca. 50% of the pore surface area after grafting. In the NHY system, there is surface area reduction of 90%, being pores' surface area reduction of the 95%. In this system, the pores' surface area is responsible for 79% of the specific surface area. The reduction of 95% in the pore surface area after grafting is mainly responsible for the great reduction of specific area, suggesting that the zirconocenes might be grafted inside these pores, obstructing them. In the case of the AER system, a reduction of ca. 23% in specific area and pores surface area was observed. Concerning micropore volume, a reduction after grafting was observed. Nevertheless, no trend among the systems could be established.

In the BET model, the "*C*" parameter is an indicator for the polarity of the surface [24]. The relationship between this value and the total grafted metal content is represented in Fig. 2.

According to Fig. 2, there is a trend between the increase of grafted Zr content and the increase of *C* parameter for the silica aerogel (AER) and commercial silicas (G56, G55 and

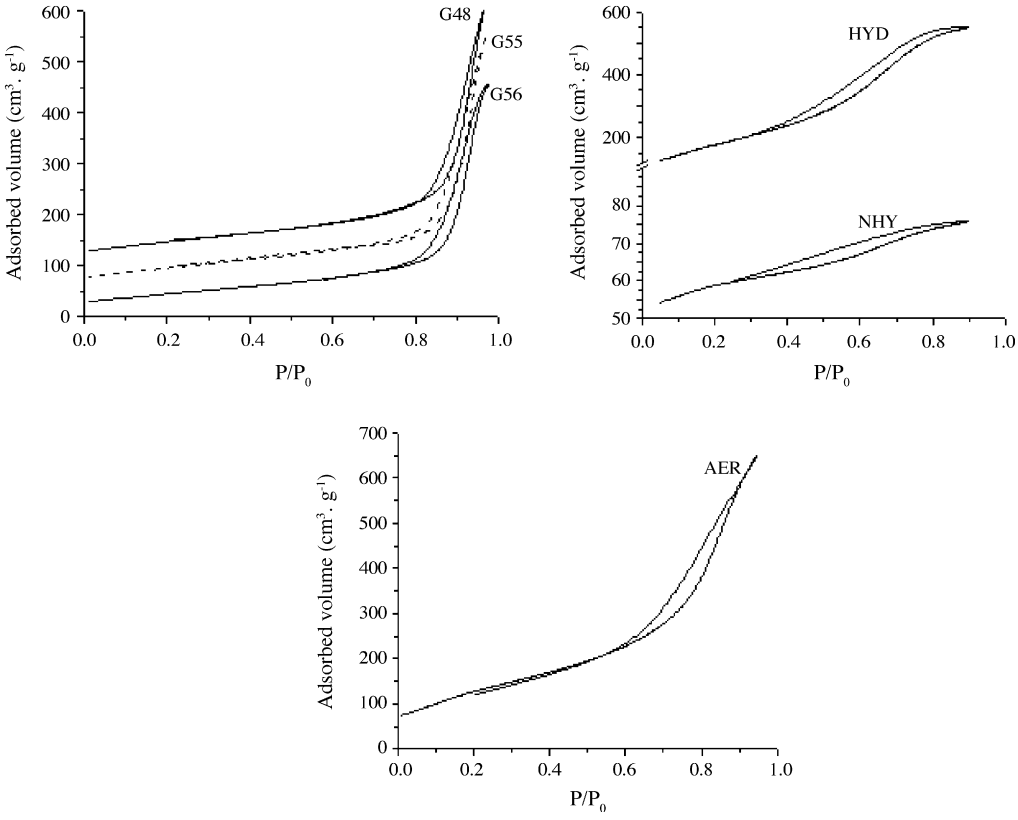

Fig. 1. Isotherms and hysteresis loops of the supported catalyst systems.

G48). However, for the xerogel NHY and HYD this trend is not observed. In NHY, the relatively high Zr content (0.4 wt.% Zr/SiO_2) grafted on the lowest surface area after the grafting ($18\ m^2\ g^{-1}$) seems to contribute to the high *C* value. Besides, such systems present ca. 13 wt.% Zr/SiO_2 from the $ZrCl_4$ employed in the synthesis.

The surface coverage concentration ($\Gamma = \mu mol\ m^{-2}$) proposed by Amati and Kováts [16], can also be correlated with the *C* parameter, as shown in Fig. 3.

According to Fig. 3, there is direct relation between Γ and *C* parameter. It is worth noting that NHY exhibits a very high *C* factor, suggesting a surface bearing high polarity. In the synthesis of such xerogels, as already mentioned, $ZrCl_4$ was employed as Lewis acid catalyst to promote the reaction between $SiCl_4$ and $Si(OEt)_4$. Residual metal catalyst might be incorporated in the silica network [12,13]. Therefore, SEM EDX analysis was performed on such a system. For comparative reasons, analyses of G48 were also performed (Table 4).

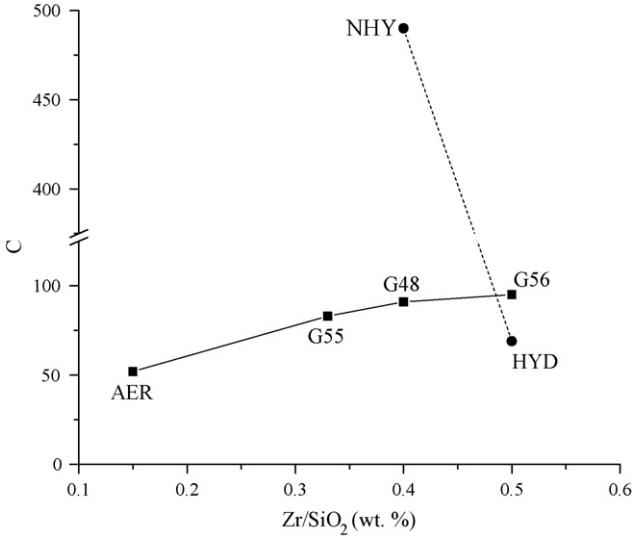

Fig. 2. Relation between grafted metal content loading and the BET *C* parameter.

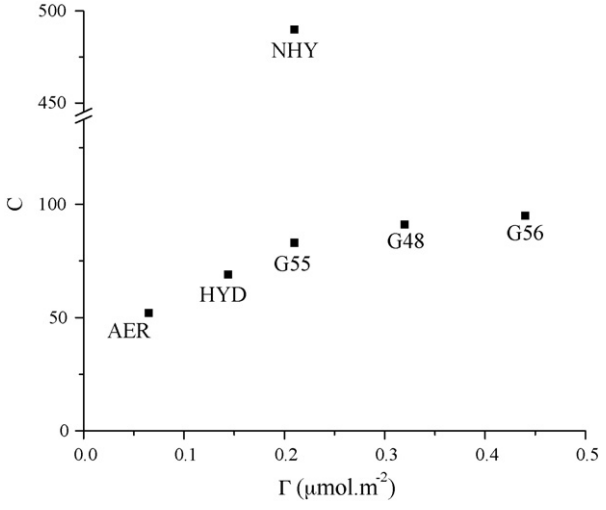

Fig. 3. Dependence of support surface polarity (*C* parameter) on the surface coverage concentration.

Table 3
Nitrogen adsorption properties of the systems before and after grafting

Before grafting						After grafting					
Silica	Specific surface area ($m^2\,g^{-1}$)	Mesopore surface area ($m^2\,g^{-1}$)	Micropore surface area ($m^2\,g^{-1}$)	Micropore volume ($cm^3\,g^{-1}$)	Pore diameter (Å)	Catalytic system	Specific surface area ($m^2\,g^{-1}$)	Mesopore surface area ($m^2\,g^{-1}$)	Micropore surface area ($m^2\,g^{-1}$)	Micropore volume ($cm^3\,g^{-1}$)	Pore diameter (Å)
G 956	210 ± 3.3	158	52	0.0226	271	G56	200 ± 2.5	155	45	0.0187	145
G 955	260 ± 3.9	206	54	0.0230	238	G55	244 ± 1.9	201	43	0.0161	128
G 948	263 ± 4.1	216	47	0.0242	279	G48	249 ± 2.6	230	19	0.0011	118
Hydrolitic	650 ± 2.0	2	648	0.6970	52	HYD	341 ± 0	3	338	0.4430	39
Non-hydrolitic	193 ± 10.3	41	152	0.0728	38	NHY	18 ± 0.4	11	7	0.0029	36
Aerogel	601 ± 2.8	3	598	0.4300	78	AER	462 ± 1.9	2	460	0.3220	58

Table 4
Zr content distribution in NHY and G48 supported catalysts determined by SEM-EDX

Spots	Zr (wt.%)	
	NHY	G48
1	30.1	5.9
2	33.2	5.5
3	25.4	6.3
4	32.2	6.1

In the NHY system, a great amount of Zr on the surface was found with relatively homogeneous distribution. However, in sample G48 the amount of Zr was roughly 6 wt.% Zr/SiO_2. Such results explain the high *C* constant value obtained for NHY.

Atomic force microscopy (AFM) is a complementary technique that assists the surface characterization of micropores and mesopores materials. It has been employed for the determination of particle size and of the degree of surface roughness of silicas [25]. In the case of the present supported catalysts, the AFM images complement the results obtained by the nitrogen adsorption, through the elucidation of the shape of the entrances of pores, their dimensions, relief type (with slits or holes and morphology of the particles).

For the catalysts supported on the commercial G55 and G48 silicas (Fig. 4), the AFM images show the homogeneity in the shape of grain and pores. The mesopores in these systems are observed in the form of slit-shaped pores, located in the width range of 130 Å, confirming measurements determined by BET method (see Table 3).

For the catalysts supported on the silicas obtained by the sol–gel method, HYD and NHY, the images are very clarifying (Fig. 5). The system HYD, with higher surface area, presents a rough surface composed by small particles, having mesopores with diameter in the range of 50 Å, while NHY is composed of great particles with less uneven surface, justifying the lowest surface area determined by the BET method. According to AFM measurements, pore diameter is around 40 Å (close to 38 Å determined by the BET method), probably resulting from the slits between grains.

AER catalyst (Fig. 6) showed a different profile: great amount of small fragments around the larger fragments. This affords a great amount of particles and slits which increase in the surface area, in spite of the mesopores size being in the range of 80 Å.

3.1. Catalyst activity in ethylene polymerization

3.1.1. Effect of the nature of silica on catalyst activity

The silicas employed in the presented study belong to three groups, according to the method of synthesis. The xerogels were prepared by the sol–gel method using alkoxydes as precursors and dried under normal pressure. The aerogel was also prepared by the sol–gel method but dried under supercritical conditions. The commercial silicas were also prepared by the sol–gel method but using sodium silicate, which was reacted with a mineral acid to form a sol–gel, which was further washed to remove the bulk of the product salts prior to being dried and sized. Fig. 7

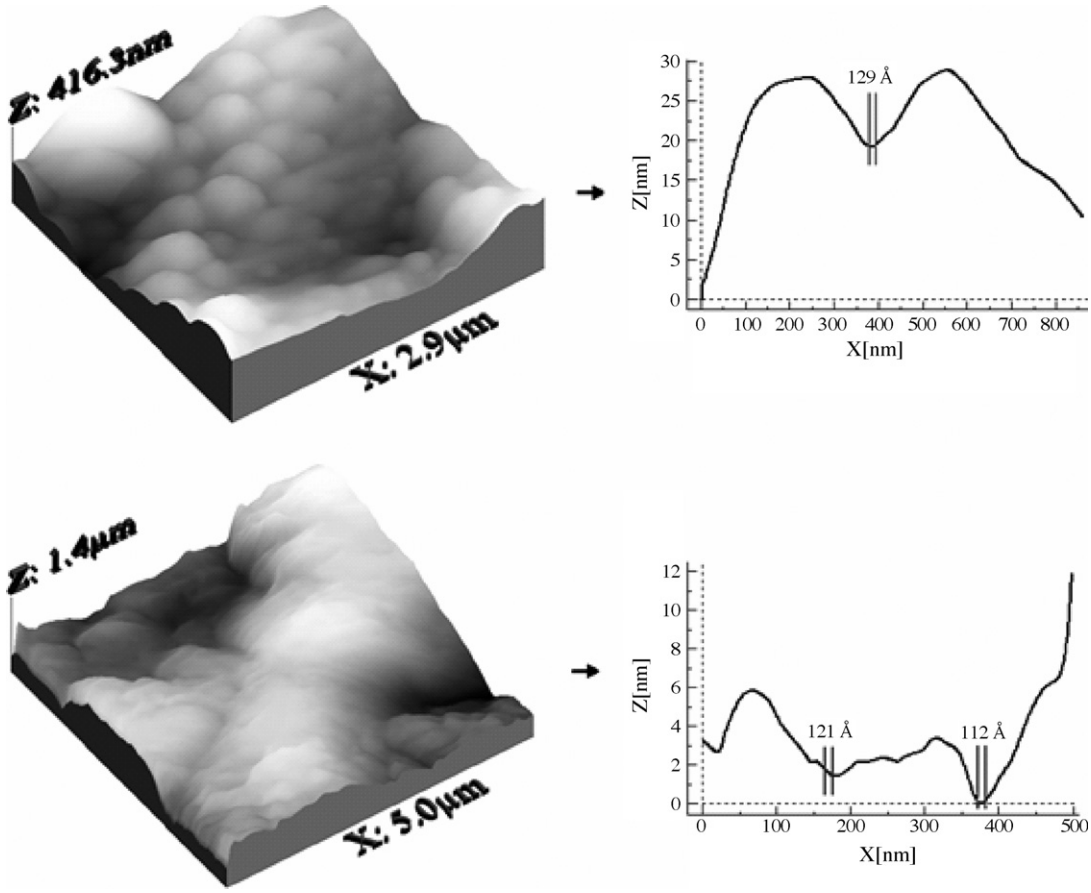

Fig. 4. AFM images of G55 sample (top) and G48 (bottom).

shows the correlation between the nature of the silica support and catalyst activity. Data are presented in the three groups. For each supported catalyst, grafted metal content was also included.

According to Fig. 7, the highest catalyst activity was obtained with the grafted catalysts using the commercial silicas Grace 956 and Grace 948 as supports, followed by that prepared with silica aerogel. The lowest catalyst activity was obtained with the supported systems grafted on the synthesized xerogels. These differences cannot be associated to the grafted metal content, since supported systems bearing the same Zr content (compare, for instance G48 and NHY) exhibit completely opposite behavior in terms of polymerization activity.

Iler [26] proposed that in silicas with pore diameter smaller than 100 Å, the negative curvature keeps silanol groups closer, favoring the formation of hydrogen bonds and therefore, increasing the stability of silanol groups against dehydroxylation (Scheme 1).

The proximity of silanol groups may promote the generation of bidentate species, which are know to be inactive for polymerization. Such phenomenon has already been reported in the literature on the investigation of the effect of silica thermal treatment (and therefore of silanol density) on zirconocene grafted content and on catalyst activity. A larger number of silanol groups (achieved at lower thermal treatment) afforded higher grafted metal content but the resulting supported metallocenes were less active in ethylene polymerization [21].

According to Table 3, hydrolytic, non-hydrolytic and aerogel silicas present pore diameter less than 100 Å. The high grafted metal content observed for NHY and HYD might have engendered the generation of some bidentate species, which are not active for ethylene polymerization.

Fig. 8 shows the correlation between support pore diameter and catalyst activity.

According to these data, catalyst activity enhances as pore diameter increases, with exception of G55. Pore diameters in the range of 115–150 Å seem not to hinder monomer diffusion to the catalyst site in the first moments for further catalyst fracturing during the polymerization reaction. Similar effects were reported in the literature. Pullukat also observed a trend between catalyst

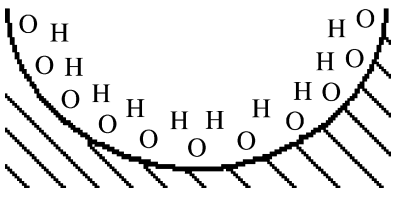

Scheme 1.

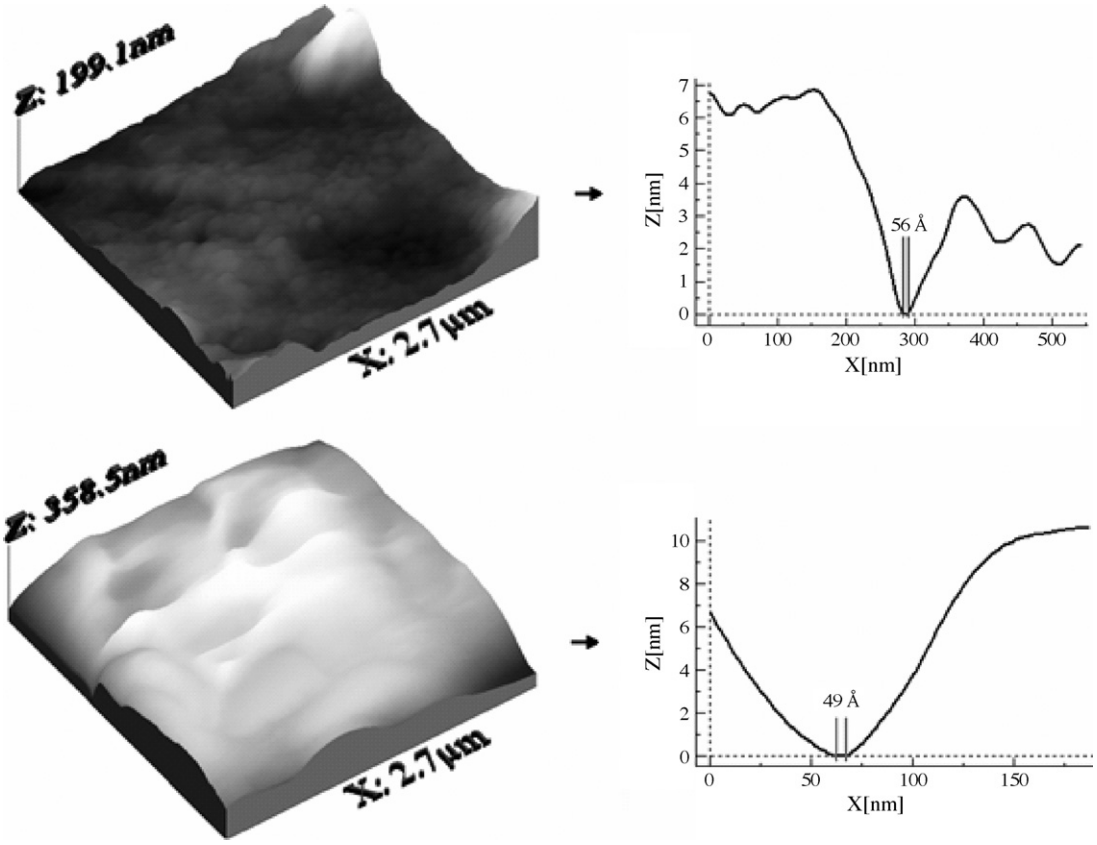

Fig. 5. AFM images of HYD sample (top) and NHY (bottom).

activity in ethylene polymerization and support pore diameter in the case of silica-supported $(BuCp)_2ZrCl_2$ [6].

3.2. Effect of the particle size on activity

Fig. 9 correlates the catalyst mean average size with catalyst activity in ethylene polymerization.

According to Fig. 9, higher catalyst activities were obtained with the systems bearing particle average size in the range of 50 μm. Particles with bigger size presented lower activity. The small-sized AER catalyst showed also a relative high catalyst activity. It is worth mentioning that such support, although AFM measurements showed two collection of particles with 0.3 and 1.6 μm, according to SAXS experiments, presented particle size close to 50 nm [14]. The effect of the catalyst size on catalyst activity was also investigated by Fink and co-workers [8]. The authors observed that smaller than 10 μm afforded better catalyst activity in ethylene polymerization. In their system, this behavior was explained in terms of more homogenous distribution of the MAO co-catalyst on the surface grain.

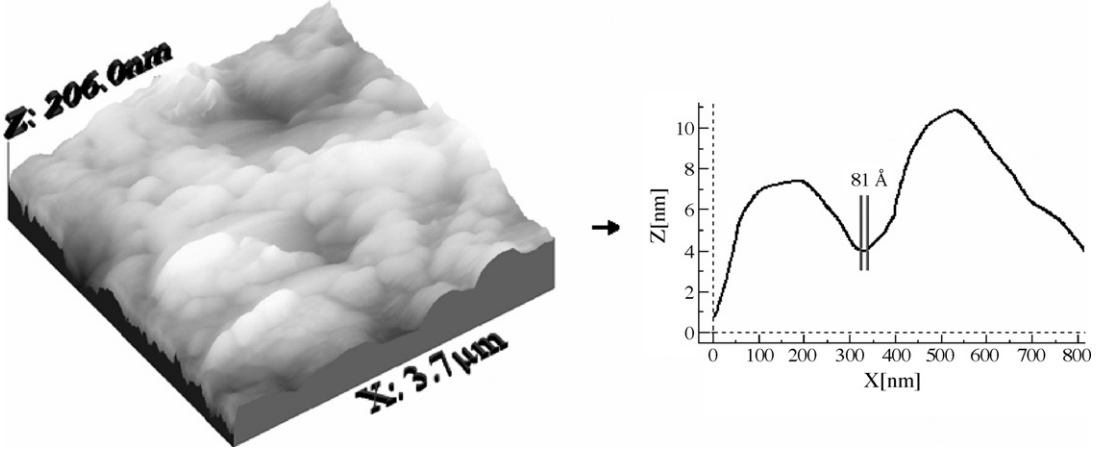

Fig. 6. AFM image of AER catalyst.

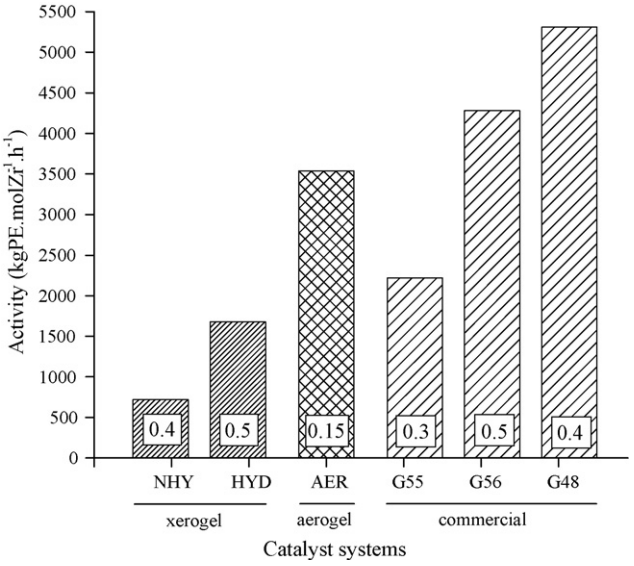

Fig. 7. Relationship between the silica nature and the activity of the catalyst system in polymerization reaction. Zr content (Zr/SiO_2 wt.%) in detail on the bars.

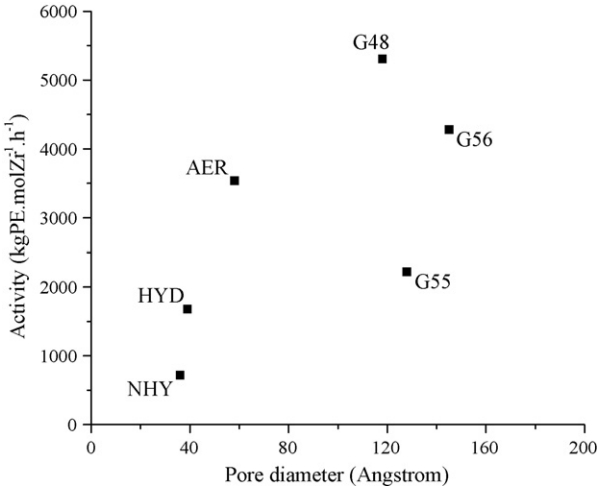

Fig. 8. Relationship between support pore diameter and catalyst activity in ethylene polymerization.

It is worth noting that NHY and HYD catalyst system present the largest particle sizes and the smallest activities in spite of the grafted metal content being close to that detected in the case of commercial supports (ca. 0.5 wt.% Zr/SiO_2). Besides, other parameters have to be taken into account, since for the commercial silicas, bearing roughly the same particle size, differences in catalyst activity might be due to grafted metal content and pore diameter.

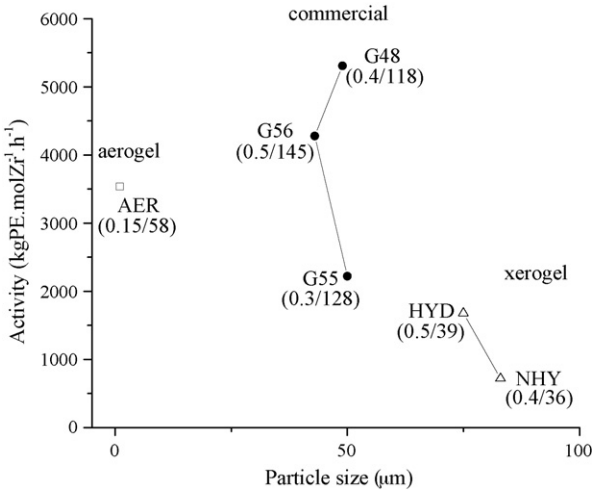

Fig. 9. Relationship between mean average catalyst diameter and catalyst activity. Grafted metal content and pore diameter between parenthesis.

3.3. Polymer characteristics

The resulting polymers were characterized by GPC and DSC. Table 5 presents molecular weight, polydispersity index (PDI), crystallinity and melting temperature. Data concerning catalyst activity were also included.

According to Table 5, molecular weight of the resulting polymers lies between 250 and 430 kg mol^{-1}. PDI was around 2.0, typical of polymers produced by single site catalysts. The broadest polydispersity was observed in the case of HYD, but the distribution was monomodal. The polymers showed similar melting temperature (around 134 °C) and crystallinities between 47 and 66%.

No clear trend between the nature of the silica or surface coverage (Γ) with Mw could be evidenced. For instance, for the commercial silicas, higher activity afforded polymers with lower Mw, while for the xerogel systems, the opposite was observed. Nevertheless, Mw of the resulting polymers seems to be influenced by catalyst pore diameter, as shown in Fig. 10.

According to Fig. 10, for each family of silica support, as catalyst pore diameter increases, polymer Mw enhances. The presence of wide open or slit-shaped pores on the catalyst surface

Table 5
Catalyst activity and polymer properties of the resulting polyethylene

System	Activity (kg PE mol Zr^{-1} h^{-1})	Mw (kg mol^{-1})	PDI	χ (%)	T_m (°C)
G56	4280	423	2.0	66	135
G55	2220	338	2.1	50	134
G48	5310	258	1.9	60	134
HYD	1680	356	3.0	47	134
NHY	720	306	2.4	55	134
AER	3537	343	2.0	53	134

[Zr] = 10^{-5} mol L^{-1}, [Al/Zr] = 1000; V = 0.15 L (toluene); P = 1 bar (ethylene); T = 60 °C; t = 30 min.

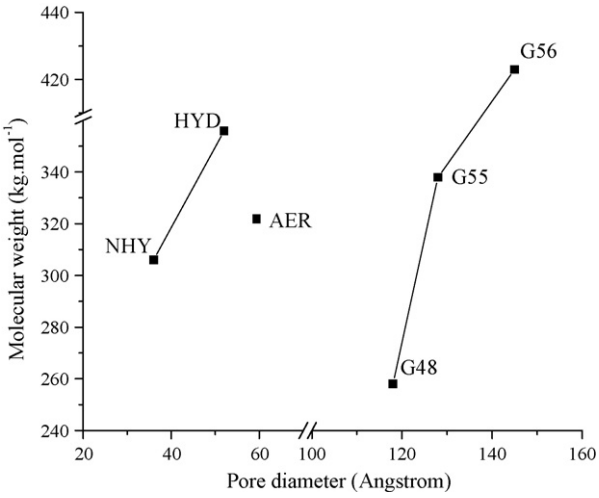

Fig. 10. Influence of the pore diameter on the molecular weight.

seems to guarantee monomer diffusion during polymer chain growth. Similar trends have already been reported in the literature, where the larger the average pore sizes of the silica support, the higher the polymer melt index [6].

4. Conclusions

Textural properties of silica support were shown to influence several parameters and properties of supported metallocene catalysts. The particle size influences on catalytic activity. Low grafted metal content and very active systems can be obtained with silica aerogel. Nevertheless, better catalyst activity was obtained with commercial silica, probably due to a more suitable and uniform particle size. Synthesized sol–gel silicas, produced either by hydrolytic or non-hydrolytic routes, did not afford any advantage in terms of catalyst activity, polymer characteristics or even polydispersity. By the way, even the likely heterogeneity of the synthesized xerogel was not enough to afford an heterogeneity of the catalyst surface species capable to produce polymers with bimodal distribution, although supported zirconocene systems HYD and NHY have showed the largest polydispersity.

Acknowledgments

We thank Ipiranga Petroquímica for GPC analysis. The research was supported by CNPq.

References

[1] J.R. Severn, J.C. Chadwick, R. Duchateau, N. Friderichs, Chem. Rev. 105 (2005) 4073.
[2] J.D. Kim, J.B.P. Soares, J. Polym. Sci., Polym. Chem. 38 (2000) 1427.
[3] J.H.Z. dos Santos, A.E. Gerbase, K.C. Rodenbusch, G.P. Pires, M. Martinelli, K. Bichinho, J. Mol. Catal. A: Chem. 184 (2002) 167.
[4] F. Silveira, S.R. Loureiro, G.B. Galland, F.C. Stedile, J.H.Z. dos Santos, T. Teranishi, J. Mol. Catal. A: Chem. 206 (2003) 389.
[5] S.R. Rodrigues, F. Silveira, J.H.Z. dos Santos, M.L. Ferreira, J. Mol. Catal. A: Chem. 206 (2004) 19.
[6] T.J. Pullukat, Effect of silica supports on olefin polymerization catalyst performance, in: M. Terano, T. Shiono (Eds.), Future Technology for Polyolefin and Olefin Polymerization Catalysis, Technology and Education Publishers, Tokyo, 2002, p. 147.
[7] D. Harrison, I.M. Coulter, S. Wang, S. Nistala, B.A. Kuntz, M. Pigeon, J. Tian, S. Collins, J. Mol. Catal. A: Chem. 128 (1998) 65.
[8] C. Pryzbyla, J. Zechlin, B. Steinmetz, B. Tesch, G Fink, in: W. Kaminsky (Ed.), Metalorganic Catalysts for Synthesis Polymerization, Springer, Berlin, 1999, pp. 321–332.
[9] J.H.Z. dos Santos, S. Dorneles, F.C. Stedile, J. Dupont, M.C. Forte, I.J.R. Baumvol, Macromol. Chem. Phys. 198 (1997) 3529.
[10] T. Kawaguchi, K. Ono, J. Non-Cryst. Solids 121 (1990) 383.
[11] B. Karmakar, G. De, D. Ganguli, J. Non-Cryst. Solids 272 (2000) 119.
[12] J. Hay, H. Raval, J. Sol–gel Sci. Tech. 13 (1998) 109.
[13] L. Bourgel, R.J.P. Curriu, D. Leclercq, P.H. Mutin, A. Vioux, J. Non-Cryst. Solids 242 (1998) 81.
[14] A. Rigacci, F.E. Dolle, E. Geissler, B. Chevalier, H. Sallée, P. Achard, O. Barbieri, S. Berthon, F. Bley, F. Livet, G.M. Pajonk, N. Pinto, C. Rochas, J. Non-Cryst. Solids 285 (2001) 187.
[15] F.C. Stedile, J.H.Z. dos Santos, Phys. Stat. Sol. 173 (1999) 123.
[16] D. Amati, E. Kováts, Langmuir 3 (1987) 687.
[17] A. Morow, Stud. Surf. Sci. Catal. A 57 (1990) A161.
[18] R. Guimarães, F.C. Stedile, J.H.Z. dos Santos, J. Mol. Catal. A: Chem. 206 (2003) 353.
[19] S. Ogasawara, Shokubai 18 (1976) 124.
[20] H.E. Bergna, Colloid chemistry of silica: an overview, in: H.E. Bergna, W.O. Roberts (Eds.), Colloid Silica: Fundamentals and Applications, Taylor and Francis, Boca Raton, 2006, p. 9.
[21] A.P. Legrand, H. Hommel, A. Tuel, A. Vidal, H. Balard, E. Papirer, P. Levitz, M. Czernichowski, R. Erre, H. Van Damme, J.P. Gallas, J.F. Hemidy, J.C. Lavalley, O. Barres, A. Burneau, Y. Grillet, Adv. Colloid Interf. Sci. 33 (1990) 91.
[22] S. Lowell, J.E. Shields, M.A. Thomas, M. Thommes, Characterization of Porous Solids and Powers: Surface Area, Pore Size and Density, Kluwer Academic Publishers, Dordrecht, The Netherlands, 2004.
[23] U. Schubert, N. Hüsing, Angew. Chem. Int. Ed. 37 (1998) 22.
[24] K.W. Lowen, E.C. Broge, J. Phys. Chem. 65 (1961) 16.
[25] J.I. Paredes, A. Martínez-Alonso, J.M.D. Tascón, Micropor. Mesopor. Mater. 65 (2003) 93.
[26] R.K. Iler, The Chemistry of Silica, Wiley Interscience Publication, John Wiley & Sons, New York, USA, 1979.